Hindawi
Journal of Nanomaterials
Volume 2019, Article ID 9734807, 11 pages
https://doi.org/10.1155/2019/9734807

Research Article

Theoretical Investigation on Failure Strength and Fracture Toughness of Precracked Single-Layer Graphene Sheets

Xin-Liang Li and Jian-Gang Guo

Tianjin Key Laboratory of Modern Engineering Mechanics, School of Mechanical Engineering, Tianjin University, Tianjin 300072, China

Correspondence should be addressed to Jian-Gang Guo; guojg@tju.edu.cn

Received 16 July 2018; Revised 20 November 2018; Accepted 20 December 2018; Published 14 February 2019

Academic Editor: Ovidiu Ersen

Young's modulus, failure strength, and failure strain of precracked graphene are investigated via finite element method based on molecular structure mechanics in this research. The influence of distribution, length, and orientation of precrack and graphene sizes on these mechanical properties is analyzed. The ratio of precrack length and graphene width is defined as P value, and its particular value P_c can be found, at which the variation trends of Young's modulus, failure strength, and strain have changes with increasing P value. In addition, the fracture toughness of precracked graphene is investigated, and the stress intensity factor (SIF) is calculated according to the Griffith criterion in classical fracture mechanics. The numerical values of the SIF are about 3.20-3.37 MPa$\sqrt{\text{m}}$, which are compared with the experimental results, and the simulations verify the applicability of the classical fracture mechanics to graphene.

1. Introduction

Pristine graphene, the two-dimensional material composed of carbon atoms, possesses superior mechanical, electronic, and thermal properties [1], so it has been applied in lots of fields, such as nanocomposites [2, 3], nanoelectronics [4, 5], and water desalination devices [6, 7]. Although graphene has many applications, it tends to fail in a brittle manner. This nature will lead to low fracture toughness [8]. In addition, the large-size graphene will inevitably introduce defects such as vacancy defects, wrinkles, and cracks in the process of manufacturing [9, 10]. Lots of researches show that cracks have significant influence on the fracture properties of a material. Therefore, it is important to explore the effect of cracks on fracture mechanical properties of graphene for its application.

Up to now, many experiments and simulations have been carried out to investigate the fracture mechanical properties of precracked graphene. Na et al. [10] performed in situ tensile experiments on copper covered by graphene to investigate the effect of tensile force on the mechanical properties of graphene. They reported that cracks of graphene are perpendicular to the loading direction, and the distance between cracks decreased with increasing strain. Zhang et al. [11] investigated the fracture toughness of graphene by in situ tensile experiments. They found that precracked graphene was a brittle material, and it was difficult to observe the process of crack propagation because of extreme fracture speed in experiment. Due to the limitation of nanoscale material, it is still a big challenge for precise experiments of graphene. Therefore, numerical simulation methods are proposed to investigate fracture properties of graphene. Based on molecular dynamics (MD) simulations, Xu et al. [12] investigated fracture mechanical properties of vacancy-defected graphene. They found that the failure strength and strain varied with the density of vacancy defects. Ansari et al. [13] investigated the effects of Stone-Wales and single vacancy defects on the mechanical properties of graphene sheets by MD

simulations. They found that two types of defects significantly decreased the failure strength and strain of graphene. Wang et al. [14] performed MD simulations under different temperatures for investigating the effect of temperature on the failure strength. They reported that the failure strength decreased with increasing temperature. Baykasoglu and Mugan [15] investigated the fracture properties of single-layer graphene via finite element method. They found that the vacancy defects and nonlinear geometric effects significantly affected the fracture performance of graphene. Xiao et al. [16] predicted fracture and progressive failure of defective graphene sheets containing a Stone-Wales defect via finite bond element method based on molecular mechanics. They reported that the failure pattern of graphene showed diagonal crack paths. Zhang et al. [17] predicted the instability of crack propagation via finite element method based on molecular structural mechanics. They reported that the loading strain rates could influence fracture properties of graphene. Xu et al. [18] investigated the effect of various tilt grain boundaries on failure strength and strain of graphene based on molecular structural mechanics. Besides the above researches, lots of efforts have been made to investigate the fracture toughness of graphene. Zhang et al. [19] investigated the fracture toughness of graphene under coupled loading via MD simulations. They reported that the stress intensity factor (SIF) of precracked graphene was 2.63-3.38 MPa$\sqrt{\text{m}}$. Datta et al. [20] also studied the SIF of precracked graphene. They reported that the SIF was 3.10-3.80 MPa$\sqrt{\text{m}}$ and 2.60-3.10 MPa$\sqrt{\text{m}}$ for armchair and zigzag graphene, respectively.

It is known to all that graphene is a kind of nanoscale material and has a discrete structure. So its cracks are not the same as macroscopic cracks. Although the effect of cracks on fracture properties of graphene has been extensively studied, crack length is relatively short in previous literature [14, 19, 20]. And the effects of distribution and length of precrack on the mechanical properties of graphene are still not systematically investigated. Molecular structural mechanics [21], an efficient and simple method, is developed to study the elastic and fracture properties of graphene [16, 22–24]. Hence, Young's modulus, failure strength, and failure strain of precracked graphene are investigated by molecular structural mechanics at present work. Simultaneously, the effects of distribution, length, and orientation of precrack and graphene sizes on these mechanical properties are systematically analyzed. In addition, the fracture toughness of precracked graphene is investigated, and the stress intensity factor (SIF) is calculated according to the Griffith criterion, and the influence of crack orientation on the SIF is also analyzed.

2. Modelling and Methods

Pristine graphene is a kind of two-dimensional material composed of carbon atoms and C-C covalent bonds. According to molecular structural mechanics [21], single-layer graphene sheets are considered as an equivalent spatial framework structure. The covalent bonds and carbon atoms of graphene are replaced by the equivalent beam elements and nodes, respectively. The atomic potential energy of graphene can be expressed by the steric potential energy, and the steric energy mainly includes bond stretching, bond angle bending, dihedral angle torsion, and out-of-plane torsion [21]. The expressions of potential energy can be written as

$$\begin{aligned} U_r &= \frac{1}{2}k_r(r-r_0)^2 = \frac{1}{2}k_r(\Delta r)^2, \\ U_\theta &= \frac{1}{2}k_\theta(\theta-\theta_0)^2 = \frac{1}{2}k_\theta(\Delta\theta)^2, \\ U_\tau &= U_\phi + U_\omega = \frac{1}{2}k_\tau(\Delta\phi)^2, \end{aligned} \tag{1}$$

where U_r, U_θ, U_ϕ, and U_ω are the atomic potential energy related to bond stretching, bond angle bending, dihedral angle torsion, and out-of-plane torsion, respectively. U_τ is the sum of atomic potential energy related to torsion. k_r, k_θ, and k_τ represent force constant related to bond stretching, bond angle bending, and bond twisting, respectively. Δr, $\Delta\theta$, and $\Delta\phi$ are an increment of the bond length, the bond angle, and angle of bond twisting, respectively. For uniaxial tensile deformation of graphene, the influence of potential energy related to dihedral torsion and out-of-plane torsion is small. Therefore, in this paper, the atomic potential energy is simplified into the sum of bond stretching potential energy and bond angle bending potential energy.

The strain energy of the beam element is equivalent to the atomic potential energy so that the cross-sectional parameters of the beam element can be obtained. In previous literature [15, 21], the beam element with circular cross section was used, and the final equations could be written as

$$\begin{aligned} \frac{EA}{L} &= k_r, \\ \frac{EI}{L} &= k_\theta, \\ \frac{GJ}{L} &= k_\tau, \end{aligned} \tag{2}$$

where E and G are the elastic modulus and shear modulus, I and J represent the moments of inertia and polar moment of inertia, A is the area of the cross section, and L is the length of the beam element. However, in this method, the different beam element cross-sectional parameters can be obtained for different force constants, and the beam element has the same in-plane and out-of-plane flexural rigidities. In order to solve these problems, in this paper, the C-C covalent bond is equivalent to the beam element with rectangular section based on modified molecular structural mechanics [25]. Therefore, the equivalent beam element has different in-plane and out-of-plane flexural rigidities, i.e., EI_z and EI_y. Detailed derivation process can be written as [25]

$$
\begin{aligned}
&L = 0.1421\ \text{nm},\\
&A = b \times h,\\
&I_y = \frac{\left(b \times h^3\right)}{12},\\
&I_z = \frac{\left(b^3 \times h\right)}{12},\\
&J = I_y + I_z,\\
&G = \frac{E}{(2(1+\mu))},
\end{aligned}
\tag{3a}
$$

$$
\begin{aligned}
&\frac{EA}{L} = 731\ \text{nN/nm},\\
&\frac{EI_z}{L} = 0.677\ \text{nN} \cdot \text{nm},\\
&\frac{EI_y}{L} = 0.267\ \text{nN} \cdot \text{nm},\\
&\frac{GJ}{L} = 0.151\ \text{nN} \cdot \text{nm},
\end{aligned}
\tag{3b}
$$

where b and h are the width and height of the beam element, respectively, I_y and I_z represent the moments of inertia, and μ is the Poisson ratio. The cross-sectional parameters of the beam element are listed in Table 1. It can be seen from the parameters in Table 1 that the Timoshenko beams [26] (beam188 element in ANSYS 12.0) are more suitable for the simulation of this work.

The nonlinear effect of the C-C covalent bond plays an important role in the process of simulation. Therefore, the modified Morse potential is used for describing the potential energy of the C-C covalent bond [27, 28]:

$$U = U_r + U_\theta, \tag{4}$$

$$U_r = D_e\left[\left(1 - e^{-\beta(r-r_0)}\right)^2 - 1\right], \tag{5}$$

$$U_\theta = \frac{1}{2}k_\theta(\theta - \theta_0)^2\left[1 + k_{\text{sextic}}(\theta - \theta_0)^4\right], \tag{6}$$

where r and θ are the current bond length and angle of the adjacent bond, respectively. Values of the parameters in equations (5) and (6) are listed in Table 2. The variations of the atomic potential energy caused by bond angle are smaller than the stretching energy [28]. For simplification, the stretching energy of bond is only considered in this paper. The stretching force of covalent bond can be derived by equation (5):

$$F = 2\beta D_e\left[1 - e^{-\beta(r-r_0)}\right]e^{-\beta(r-r_0)}. \tag{7}$$

The curve of force-strain between the C-C bonds is shown in Figure 1, where strain ε can be obtained by $\varepsilon = (r - r_0)/r_0$. Belytschko et al. [28] reported that the fracture of the C-C bonds depended primarily on the interatomic potential before the inflection point, after which, the potential was not important. It can be seen from Figure 1 that when the strain is equal to zero the beam element which represents the C-C bond is in equilibrium. As the strain increases, the inflection point occurs when the strain is equal to 19%. The nonlinear stress-strain curve of the beam element is described by $\sigma = F/A$ and equation (7).

The atomistic model with a honeycomb hexagonal structure is constructed via the above equivalent method, as shown in Figure 2, in which the lattice constant is 0.249 nm. In order to obtain a central crack of length $2a$ and perpendicular to the loading direction, the C-C bonds at defined positions (the red area in Figure 2) are deleted. In addition, L and W are the length and width of graphene, respectively. The edge effect is important for fracture properties of graphene. However, the main objective of this paper is to study the effect of precrack on the fracture properties of graphene. Thus, the edge effect is neglected. Actually, it will lose the significance of research when crack sizes are larger than $0.6W$. Therefore, only crack sizes which are below $0.6W$ are considered in this paper. In the process of simulation, the left and right edge atoms are subjected to a displacement load along the X direction; the top and bottom edge atoms are constrained along the Y direction, as shown in Figure 2. In the following simulations, this type of boundary condition is used unless otherwise specified. At present work, the dimension of atomistic models is defined as $L \times W$; they are $10 \times 10\ \text{nm}^2$, $20 \times 20\ \text{nm}^2$, $30 \times 30\ \text{nm}^2$, and $43 \times 43\ \text{nm}^2$, respectively.

3. Results and Discussion

3.1. Effective Young's Modulus of Precracked Graphene. The atomistic models with different crack distributions along the width direction are constructed by means of the method in Section 2 (as shown in Figure 3(a)). Young's modulus of pristine graphene has been studied [18]. For precracked graphene, the effective Young modulus will be researched in this paper. The effects of crack distribution along the width direction and the length of central crack on the effective Young modulus of graphene are discussed. In the process of simulation, the left end of graphene is fixed, and a displacement load ΔL is applied to the right end. The effective Young modulus can be calculated by

$$E = \frac{\sigma}{\varepsilon} = \frac{F}{Wt} \times \frac{L}{\Delta L}, \tag{8}$$

where σ and ε represent the tensile stress and strain, respectively, t is the thickness of a single-layer graphene, and $t = 0.34$ nm.

The effective Young moduli of pristine and precracked graphene are calculated, respectively, and the influence of precrack and graphene sizes is further discussed. First of all, Young's modulus of pristine graphene agrees well with the results of experiment [29], first principle calculation [30, 31], density functional calculations [32], and molecular structure mechanics [22]. The comparison between present works with those of the literature is listed in Table 3. Thus, the results are reliable in this paper.

Table 1: The cross-sectional parameters of the beam element [25].

b (nm)	h (nm)	A (nm^2)	I_y (nm^4)	I_z (nm^4)	E (TPa)	G (TPa)	J (nm^4)
0.1049	0.0678	7.11×10^{-3}	2.73×10^{-6}	6.53×10^{-6}	14.56	2.30	9.26×10^{-6}

Table 2: The parameters in modified Morse potential [27, 28].

r_0 (m)	β (m^{-1})	D_e (N·m)	θ_0 (rad)	k_θ (N·m/rad^2)	k_{sextic} (rad^{-4})
1.421×10^{-10}	2.625×10^{10}	6.03105×10^{-19}	2.094	0.9×10^{-18}	0.754

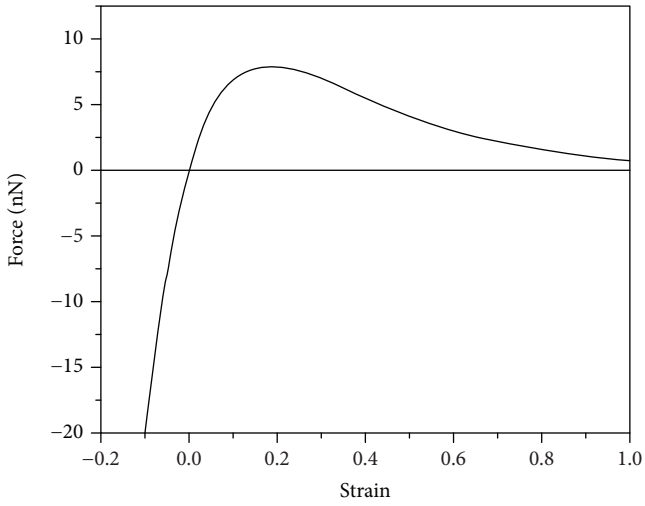

Figure 1: The curve of force-strain between the C-C bonds.

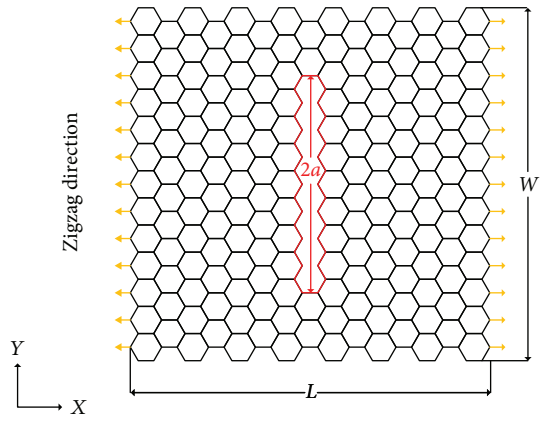

Figure 2: Schematic of precracked graphene under uniaxial tension.

For convenience, the ratio of precrack length and graphene width is defined as the P value. The variations of the effective Young modulus of pristine and precracked graphene with increasing P value are exhibited in Figure 3(b). It can be seen from this figure that the effective Young modulus of precracked graphene is lower than that of pristine graphene. For precracked graphene, its effective Young's modulus decreases with increasing P value, and the variation trends become noticeable when the P value is greater than about 0.1. What is more, it can be found from Figure 3(b) that crack distribution can also influence the effective Young modulus of precracked graphene. For the same P value, the effective Young modulus of W-1 is the lowest, and that of W-3 is the highest. That is to say, a crack has more remarkable influence than two or three cracks with the same sizes on the effective Young modulus of precracked graphene.

In addition, the precrack can also influence the size effect of Young's modulus. Figure 3(c) shows the variations of the effective Young modulus with increasing graphene length for different P values. It can be found from this figure that the effective Young modulus increases as the length of precracked graphene increases. Moreover, with the increase of the P value, the size effect of the effective Young modulus becomes more remarkable.

3.2. Failure Strength and Failure Strain of Precracked Graphene. First of all, the failure strength and strain of pristine single-layer graphene sheets are calculated to verify the reliability of the Morse potential function which describes the nonlinear behaviour of graphene. The stress-strain curves of pristine armchair and zigzag graphene under uniaxial tension are shown in Figure 4. It can be seen from this figure that the failure strength and strain of armchair graphene are larger than those of zigzag graphene. The failure strength and strain of pristine armchair and zigzag graphene are 111.9 GPa and 88.1 GPa and 0.23 and 0.22, respectively. These results agree well with the counterparts in the literature [13, 29, 30, 33]. The comparison between present works with those of the literature is listed in Table 3. Then, the failure strength and strain of precracked single-layer graphene will be calculated, and the effects of distribution, length, and orientation of precrack and graphene sizes on these properties will be analyzed.

As shown in Figure 2, uniaxial tensile loading is applied to graphene sheets with a central precrack which is perpendicular to the loading direction. Its failure strength and strain are calculated and illustrated, respectively. Figure 5 shows the variations of the failure strength and strain with increasing P value for different domain sizes. It can be seen from the figures that the failure strength and strain show a particular degrading-stabilizing trend with increasing P value. A particular value of P can be found, about 0.1, which is the same as the result in the above section, so the particular value of P can

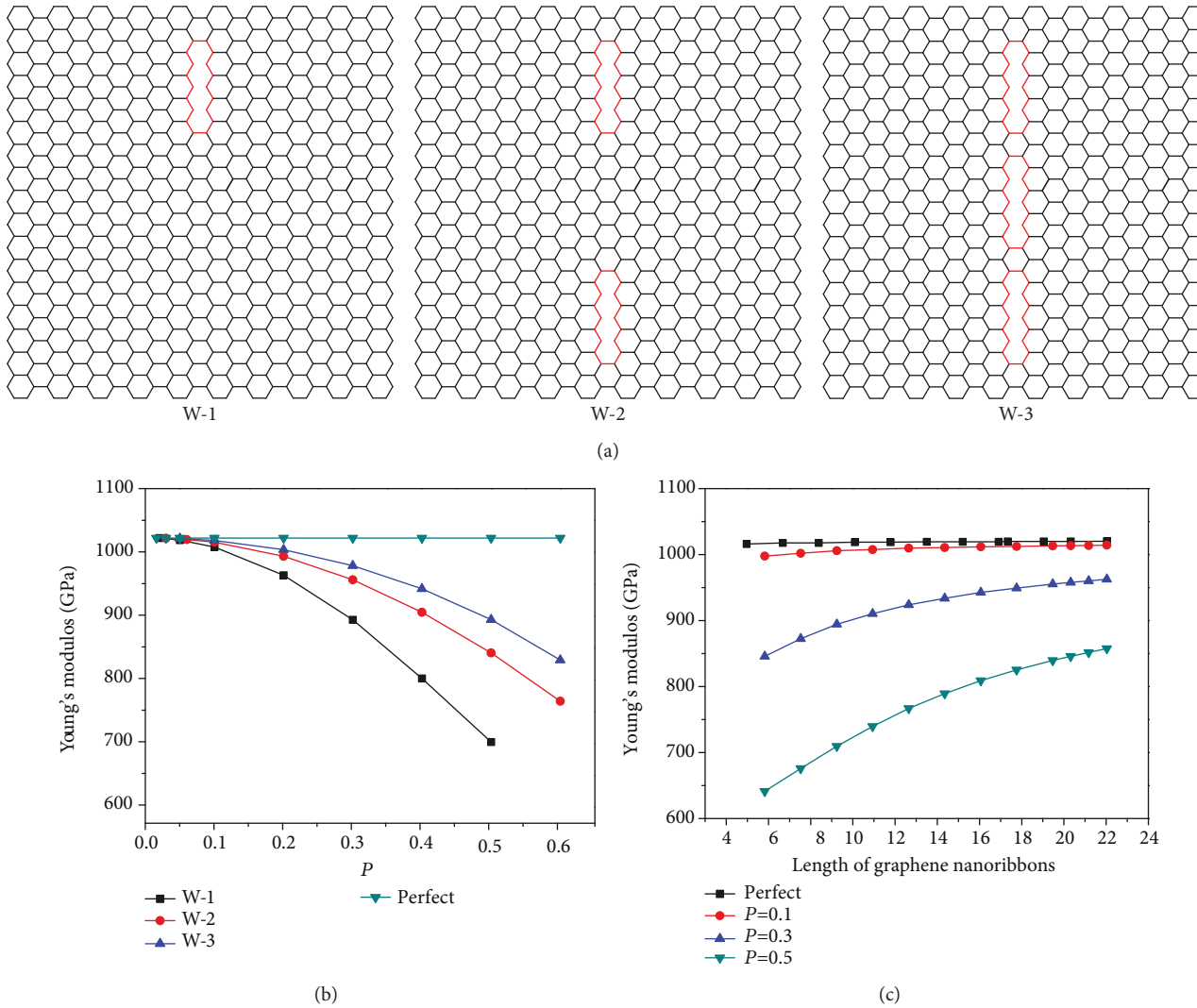

FIGURE 3: (a) The atomistic models with different crack distributions along the width direction. (b) The variations of the effective Young modulus with increasing P value for different crack distributions along the width direction. (c) The variations of the effective Young modulus with increasing graphene length for different P values.

be defined as P_c, and $P_c = 0.1$. The failure strength and strain sharply decline until the P value reaches about P_c, and then they gradually tend to be steady.

In addition, the failure strength and strain can be influenced by graphene sizes in the study of pristine graphene [34]. Similarly, the size effect can be found for a precracked graphene. When the P value is specified, it can be found from Figure 5 that the failure strength and strain of precracked graphene decrease with increasing domain size. The reason is that the absolute size of precrack increases with increasing domain size. As a result, a large precrack makes the failure of graphene more easily.

The cracks are prefabricated along the length direction and perpendicular to the loading direction. However, the distributions of these cracks can be different. They can have different distributions along the width (as shown in Figure 3(a)) and length (as shown in Figure 6(a)) directions. The different crack distributions can influence the failure strength and strain of graphene. For different crack distributions along the width direction, the variations of the failure strength and strain with increasing P value are illustrated in Figures 7(a) and 7(b), respectively. It can be seen from these figures that the failure strength and strain significantly decrease with increasing P value for each kind of crack distributions along the width direction. It is similar to those in Figure 5. Moreover, it is interesting that the failure strength and strain show an improving trend with increasing amounts of cracks along the width direction. When the P value is fixed, the failure strength and strain of W-1 are the lowest, and those of W-3 are the highest. For different crack distributions along the length direction, the variations of the failure strength and strain with increasing P value are illustrated in Figures 6(b) and 6(c), respectively. When the P value is less than P_c, the difference of failure strength and strain is negligible for three kinds of crack distributions along the length direction. However, when the P value is more than P_c,

Table 3: The comparison between present works with those of the literature (includes Young's moduli, failure strength, failure strain, and fracture toughness).

Method	Young's moduli (GPa)	Type	Failure strength (GPa)	Failure strain	Fracture toughness ($MPa\sqrt{m}$)
Experiment [11, 29]	1000 ± 100		130 ± 10	0.25	4.0
MD [19, 33]	1010 ± 30	Armchair	107	0.2	3.38
		Zigzag	90	0.13	
Ab initio calculation [30]	1050	Armchair	121	0.266	—
		Zigzag	110	0.194	
MD [20, 38]	855	—	—	—	3.1
Molecular structure mechanics [17, 22]	1040	—	—	—	3.34
MD [13, 39]	—	Armchair	127	0.22	3.2
		Zigzag	123	0.23	
Molecular structure mechanics [18]	—	Armchair	100.47	0.23	—
		Zigzag	79.82	0.22	
Theory [11]	—	—	—	—	3.2
Present works	1022.54	Armchair	111.9	0.23	3.20-3.37
		Zigzag	88.1	0.22	

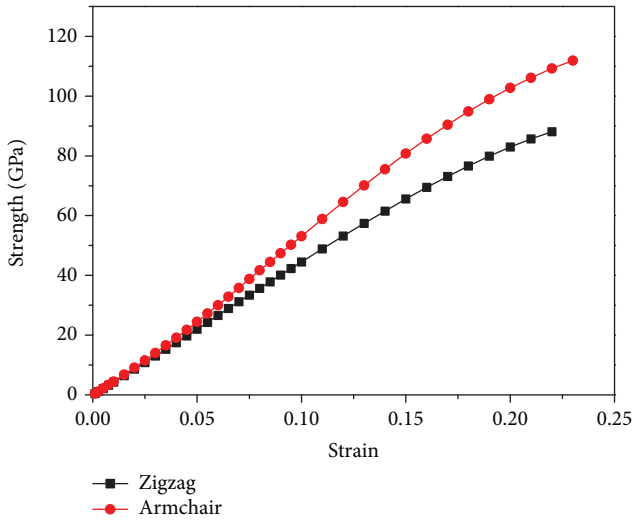

Figure 4: Stress-strain curves of pristine armchair and zigzag graphene under uniaxial tension.

it can be found that the difference becomes remarkable. Furthermore, the failure strain may go up with increasing P value for the cases of L-2 and L-3, as shown in Figure 6(c). Therefore, we can obtain an expected failure strain of graphene by designing its crack distributions.

If the precrack of graphene is not perpendicular to the loading direction but has an angle with it, three particular cases are applied to investigate the influence of crack orientation on the failure strength and strain. The atomistic models with three kinds of crack orientations are constructed, which are 30°, 60°, and 90°, respectively (as shown in Figure 8(a)). The variations of the failure strength and strain with increasing P value for three kinds of crack orientations are illustrated in Figures 8(b) and 8(c). With the increase of the P value, similar to the above discussions, the failure strength and strain sharply drop until the P value reaches about P_c, and then they gradually tend to be steady. Moreover, when the P value is fixed, failure strength and strain reduce with increasing crack orientation, i.e., the failure strength and strain of D-3 are the lowest, and those of D-1 are the highest, which is reasonable and logical.

3.3. Fracture Toughness of Precracked Graphene. Fracture toughness is one of the most important mechanical properties of a material and has been used for describing the ability of a material to resist fracture. It has been shown in literature [11] that the useful strength of graphene depends on its fracture toughness, rather than the initial strength controlled by the C-C bond cleavage. In this research, the fracture toughness of precracked graphene will be investigated by molecular structure mechanics, and stress intensity factor (SIF) will be calculated. For the plane stress problem, there are two types of SIF, i.e., mode I and mode II.

The SIF of mode I can be obtained when load direction is perpendicular to the precrack. According to the Griffith criterion in classical fracture mechanics [35–37], the stress intensity factor of mode I can be obtained:

$$K = \sqrt{2} F \sigma \sqrt{\pi a}, \tag{9a}$$

$$F = \left(1 - 0.025 f^2 + 0.06 f^4\right) \sqrt{\sec\left(\frac{\pi f}{2}\right)}, \tag{9b}$$

$$f = \frac{2a}{W}, \tag{9c}$$

where F is the correction factor, σ is the tensile stress, $2a$ is the crack length, and W is the width of graphene.

When precracked graphene (as shown in Figure 2) has different domain sizes, the variations of mode I stress

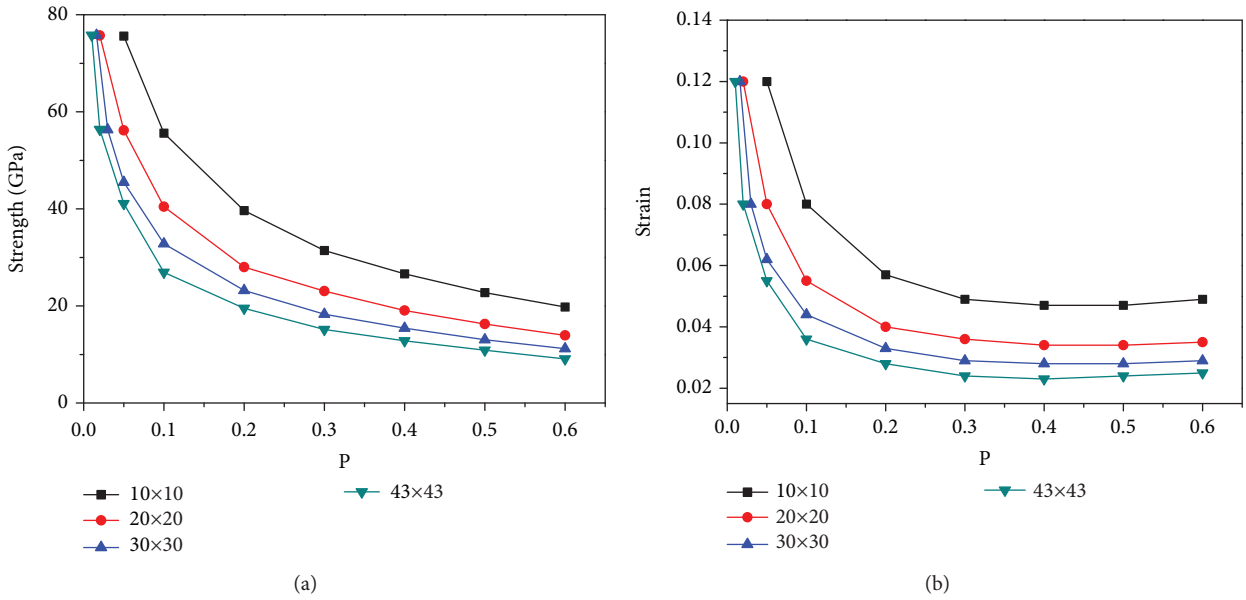

FIGURE 5: (a) The failure strength of graphene with a central precrack for different domain sizes. (b) The failure strain of graphene with a central precrack for different domain sizes.

intensity factor with increasing P value are illustrated in Figure 9. The domain size of graphene has insignificant effect on the SIF. The SIF experiences an increasing-stabilizing process with increasing P value. It increases when the P value is less than P_c and then becomes nearly constant as the P value is over P_c. The constant values of the SIF are about 3.20-3.37 MPa$\sqrt{\text{m}}$. It is consistent with the results of the literature. The comparison between present works with those of the literature is listed in Table 3. In some research works [11, 35], the applicable range of classical fracture mechanics is discussed in order to calculate fracture toughness. Zhang et al. [11] found that the classical Griffith criterion was still applicable when the crack size was as low as 33 nm. Yin et al. [35] proved that the applicable size of crack was as low as 10 nm via MD simulations. According to our research, when the P value is less than P_c, the theory of classical fracture mechanics overestimates the SIF.

The stress intensity factors of mode I and mode II both exist when load direction is not perpendicular to the precrack. According to the theory of maximum circumferential stress in classical fracture mechanics and equations (9a)–(9c), the stress intensity factor of mode I, mode II, and mixed mode can be obtained, respectively.

$$K_{\text{I}} = K \sin^2\varphi, \tag{10a}$$

$$K_{\text{II}} = K \sin\varphi \cos\varphi, \tag{10b}$$

$$K_{\text{eff}} = \sqrt{K_{\text{I}}^2 + K_{\text{II}}^2}, \tag{10c}$$

where K_{I}, K_{II}, and K_{eff} are mode I, mode II, and mixed-mode stress intensity factors, respectively, and φ is the angle between the crack and the loading direction.

When the angles between the crack and the loading direction are 30° and 60° (as shown in Figure 8(a), D-1 and D-2), the variations of the SIF with increasing P value are illustrated in Figures 10 and 11, respectively. The SIF of mode II is larger than that of mode I when the angle between the crack and the loading direction is 30°. However, they are opposite when the angle is 60°.

The variations of the SIF with increasing orientation angle of crack are illustrated in Figure 12. It can be seen from this figure that the SIF of mode I increases and that of mode II decreases with increasing angle, respectively. Moreover, the SIF of mode I is larger than that of mode II when the angle is less than 45°. However, they are opposite when the angle is more than 45°.

4. Conclusions

For the single-layer graphene sheets with various prefabricated cracks, Young's modulus, failure strength, and strain are investigated via finite element method based on molecular structure mechanics. Simultaneously, the influence of distribution, length, and orientation of precrack and graphene sizes is analyzed. The results show that these factors have significant influence on the mechanical properties of the precracked graphene. It is noteworthy that a particular value of P, $P_c = 0.1$, is found for the mechanical properties of the precracked graphene. The variation trends of the effective Young modulus, failure strength, and strain will have changes when the P value reaches P_c. In addition, the fracture toughness of precracked graphene is investigated, and its SIF is calculated according to the Griffith criterion in classical fracture mechanics. When the P value reaches P_c, the SIF keeps nearly constant. It is about 3.20-3.37 MPa$\sqrt{\text{m}}$. On the contrary, the SIF cannot keep constant and is lower than the reasonable value when the

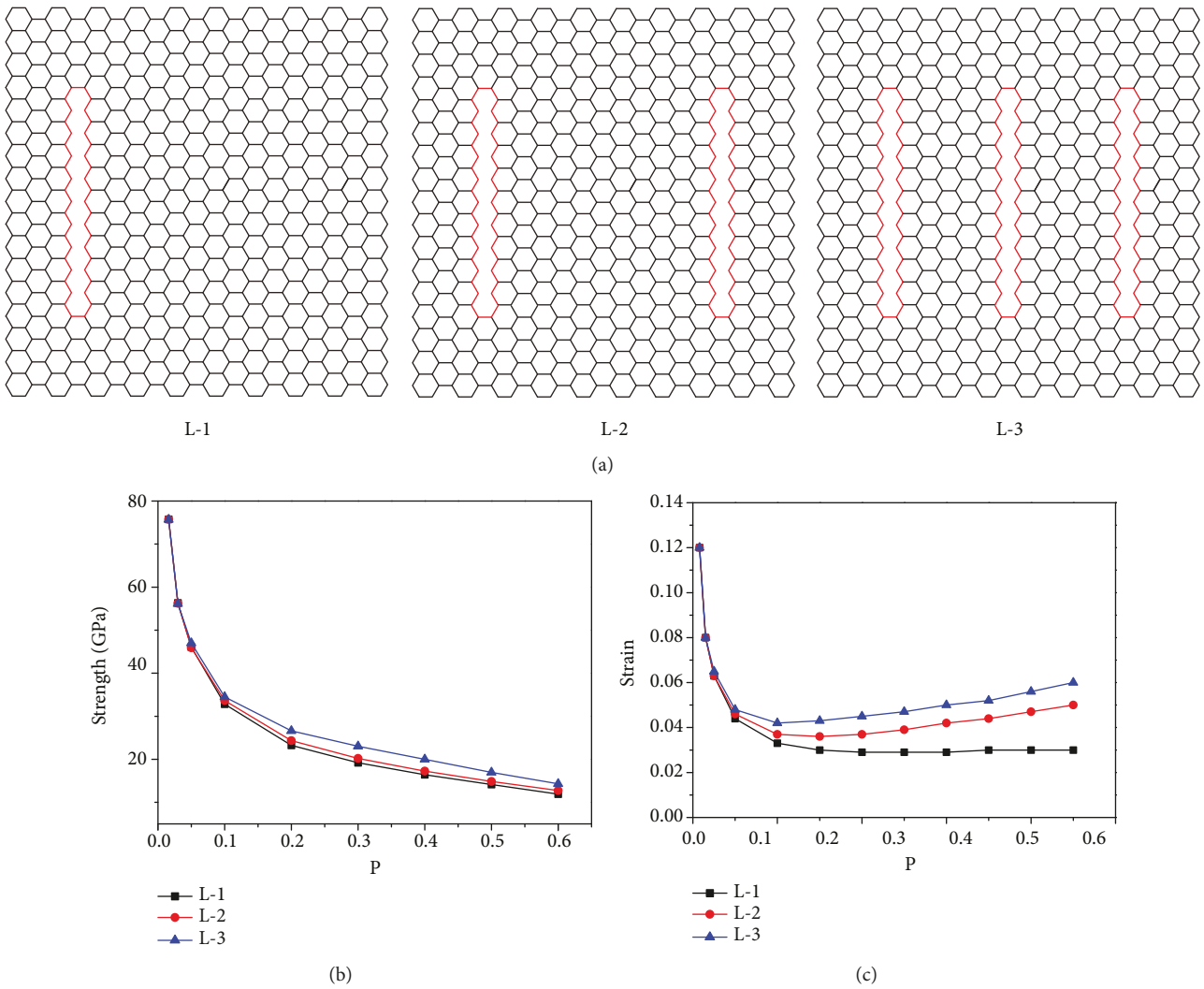

Figure 6: (a) The atomistic models with different crack distributions along the length direction. (b) The variations of the failure strength with increasing P value for different crack distributions along the length direction. (c) The variations of the failure strain with increasing P value for different crack distributions along the length direction.

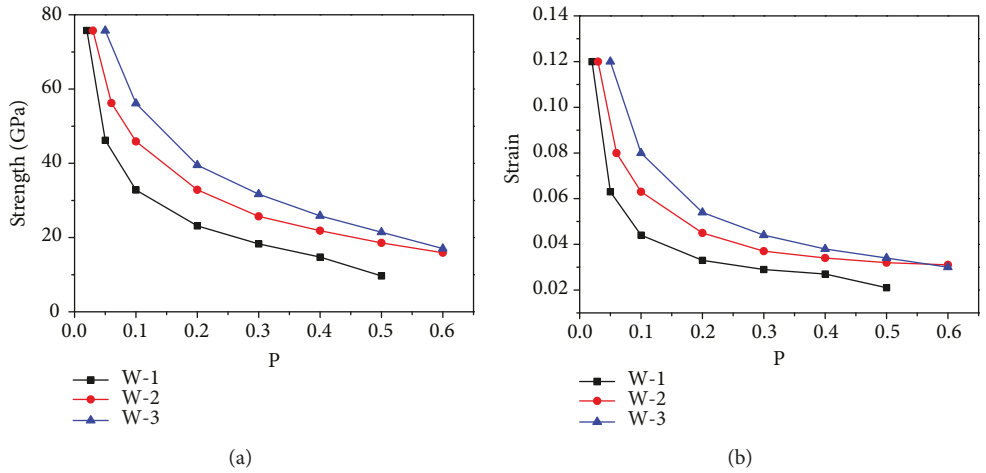

Figure 7: (a) The variations of the failure strength with increasing P value for different crack distributions along the width direction. (b) The variations of the failure strain with increasing P value for different crack distributions along the width direction.

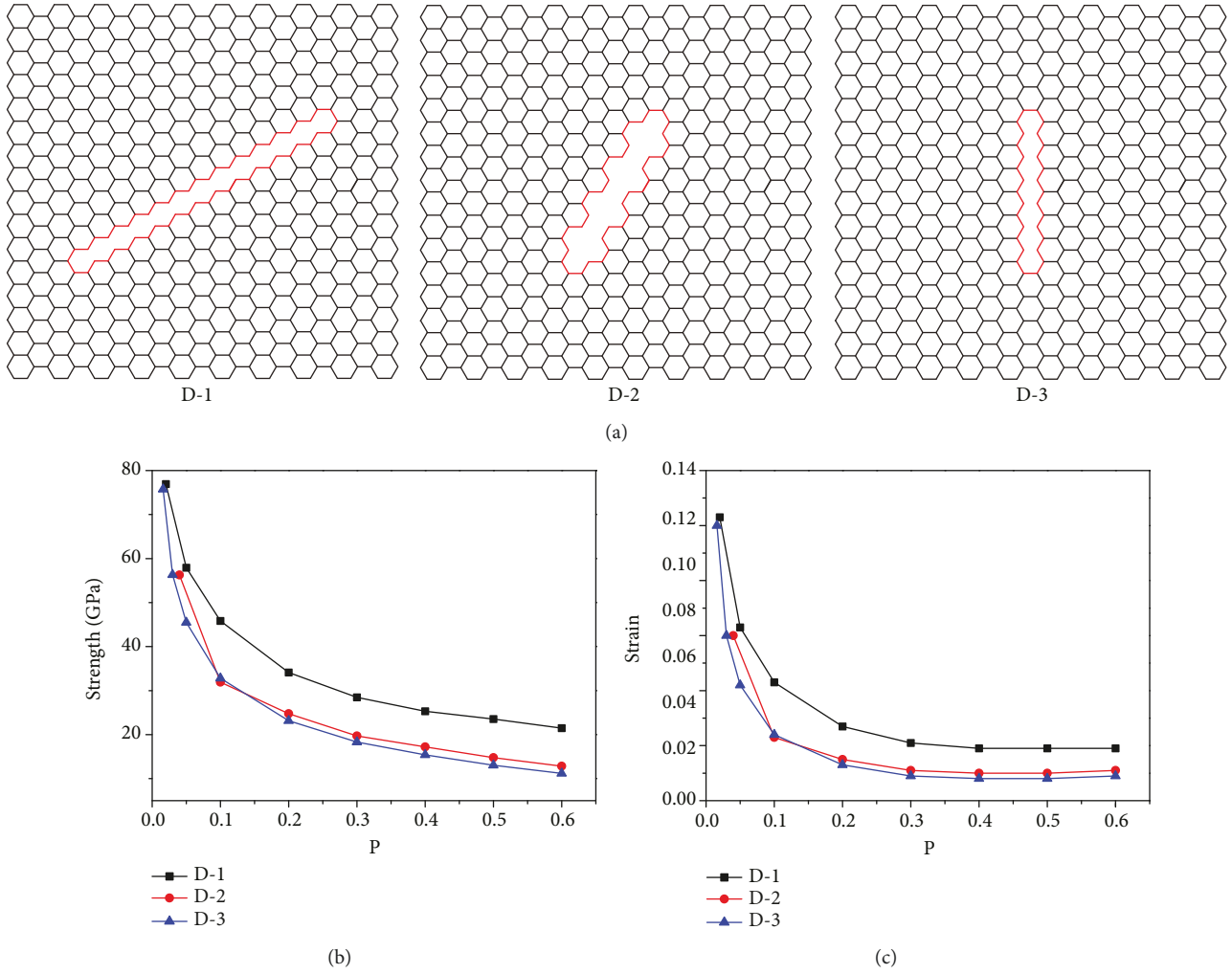

FIGURE 8: (a) The atomistic models with different crack orientations. (b) The variations of the failure strength with increasing P value for three kinds of crack orientations. (c) The variations of the failure strain with increasing P value for three kinds of crack orientations.

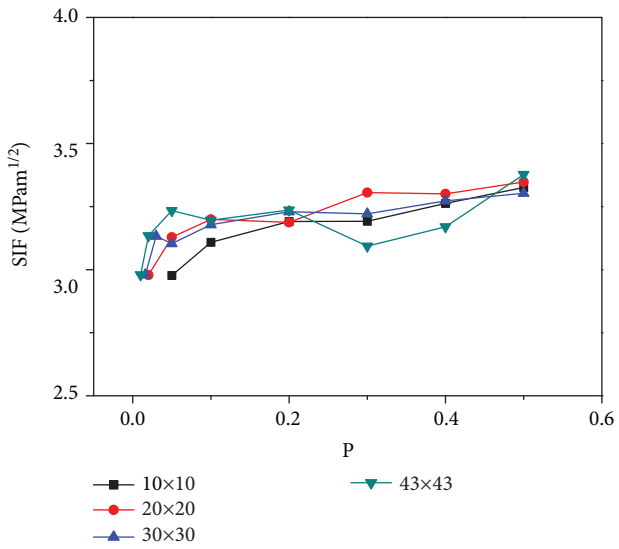

FIGURE 9: The variations of the SIF with increasing P value for different domain sizes.

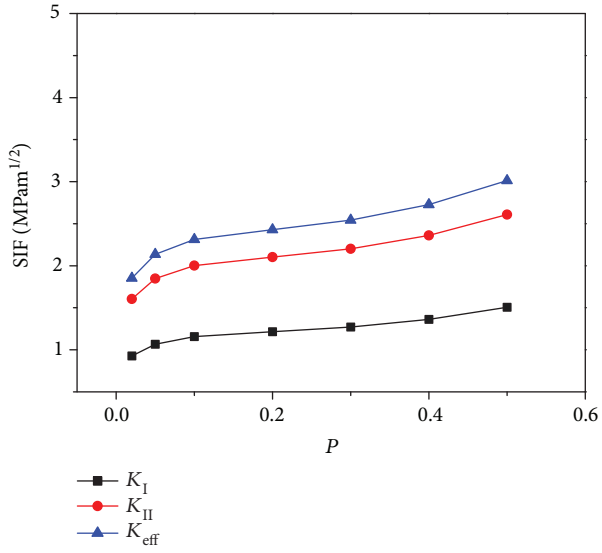

FIGURE 10: The variations of the SIF of the D-1 graphene with increasing P value.

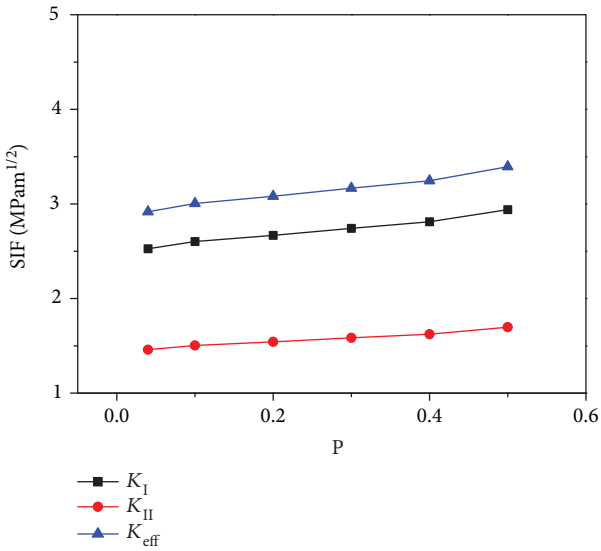

Figure 11: The variations of the SIF of the D-2 graphene with increasing P value.

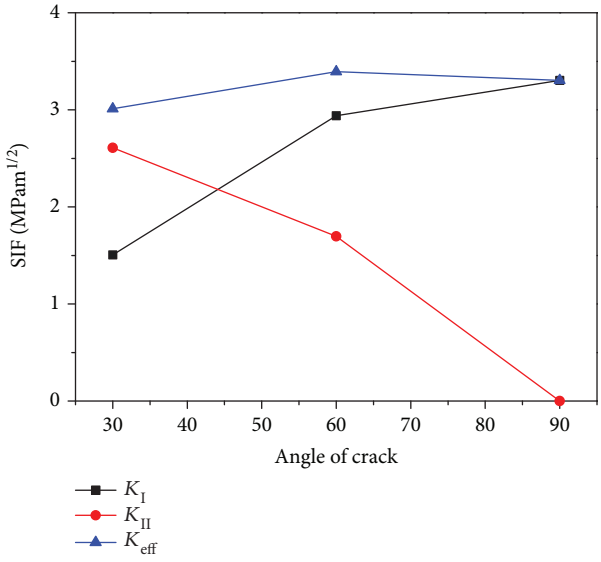

Figure 12: The influence of crack orientation on the SIF.

P value is less than P_c. Thus, the theory of classical fracture mechanics overestimates the SIF.

Data Availability

The data used to support the findings of this study are available from the corresponding author upon request.

Conflicts of Interest

The authors declare that there is no conflict of interests regarding the publication of this paper.

Acknowledgments

This work is supported by the National Natural Science Foundation of China (Grant nos. 11872268, 11890682, and 11502167).

References

[1] Y. Wang and Z. Liu, "The fracture toughness of graphene during the tearing process," *Modelling and Simulation in Materials Science and Engineering*, vol. 24, no. 8, 2016.

[2] D. A. Dikin, S. Stankovich, E. J. Zimney et al., "Preparation and characterization of graphene oxide paper," *Nature*, vol. 448, no. 7152, pp. 457–460, 2007.

[3] J. R. Potts, S. H. Lee, T. M. Alam et al., "Thermomechanical properties of chemically modified graphene/poly(methyl methacrylate) composites made by in situ polymerization," *Carbon*, vol. 49, no. 8, pp. 2615–2623, 2011.

[4] J. S. Bunch, A. M. van der Zande, S. S. Verbridge et al., "Electromechanical resonators from graphene sheets," *Science*, vol. 315, no. 5811, pp. 490–493, 2007.

[5] V. Singh, S. Sengupta, H. S. Solanki et al., "Probing thermal expansion of graphene and modal dispersion at low-temperature using graphene nanoelectromechanical systems resonators," *Nanotechnology*, vol. 21, no. 16, article 165204, 2010.

[6] D. Cohen-Tanugi and J. C. Grossman, "Water desalination across nanoporous graphene," *Nano Letters*, vol. 12, no. 7, pp. 3602–3608, 2012.

[7] S. C. O'Hern, M. S. H. Boutilier, J. C. Idrobo et al., "Selective ionic transport through tunable subnanometer pores in single-layer graphene membranes," *Nano Letters*, vol. 14, no. 3, pp. 1234–1241, 2014.

[8] C. Cao, S. Mukherjee, J. Y. Howe et al., "Nonlinear fracture toughness measurement and crack propagation resistance of functionalized graphene multilayers," *Science Advances*, vol. 4, no. 4, article eaao7202, 2018.

[9] J. C. Meyer, C. Kisielowski, R. Erni, M. D. Rossell, M. F. Crommie, and A. Zettl, "Direct imaging of lattice atoms and topological defects in graphene membranes," *Nano Letters*, vol. 8, no. 11, pp. 3582–3586, 2008.

[10] S. R. Na, X. Wang, R. D. Piner, R. Huang, C. G. Willson, and K. M. Liechti, "Cracking of polycrystalline graphene on copper under tension," *ACS Nano*, vol. 10, no. 10, pp. 9616–9625, 2016.

[11] P. Zhang, L. Ma, F. Fan et al., "Fracture toughness of graphene," *Nature Communications*, vol. 5, no. 1, p. 3782, 2014.

[12] L. Xu, N. Wei, and Y. Zheng, "Mechanical properties of highly defective graphene: from brittle rupture to ductile fracture," *Nanotechnology*, vol. 24, no. 50, article 505703, 2013.

[13] R. Ansari, S. Ajori, and B. Motevalli, "Mechanical properties of defective single-layered graphene sheets via molecular dynamics simulation," *Superlattices and Microstructures*, vol. 51, no. 2, pp. 274–289, 2012.

[14] M. C. Wang, C. Yan, L. Ma, N. Hu, and M. W. Chen, "Effect of defects on fracture strength of graphene sheets," *Computational Materials Science*, vol. 54, pp. 236–239, 2012.

[15] C. Baykasoglu and A. Mugan, "Nonlinear fracture analysis of single-layer graphene sheets," *Engineering Fracture Mechanics*, vol. 96, pp. 241–250, 2012.

[16] J. R. Xiao, J. Staniszewski, and J. W. Gillespie Jr., "Fracture and progressive failure of defective graphene sheets and carbon nanotubes," *Composite Structures*, vol. 88, no. 4, pp. 602–609, 2009.

[17] B. Zhang, H. Xiao, G. Yang, and X. Liu, "Finite element modelling of the instability in rapid fracture of graphene," *Engineering Fracture Mechanics*, vol. 141, pp. 111–119, 2015.

[18] N. Xu, J. G. Guo, and Z. Cui, "The influence of tilt grain boundaries on the mechanical properties of bicrystalline graphene nanoribbons," *Physica E: Low-dimensional Systems and Nanostructures*, vol. 84, pp. 168–174, 2016.

[19] B. Zhang, L. Mei, and H. Xiao, "Nanofracture in graphene under complex mechanical stresses," *Applied Physics Letters*, vol. 101, no. 12, article 121915, 2012.

[20] D. Datta, S. P. V. Nadimpalli, Y. Li, and V. B. Shenoy, "Effect of crack length and orientation on the mixed-mode fracture behavior of graphene," *Extreme Mechanics Letters*, vol. 5, pp. 10–17, 2015.

[21] C. Li and T. W. Chou, "A structural mechanics approach for the analysis of carbon nanotubes," *International Journal of Solids and Structures*, vol. 40, no. 10, pp. 2487–2499, 2003.

[22] A. Sakhaee-Pour, "Elastic properties of single-layered graphene sheet," *Solid State Communications*, vol. 149, no. 1-2, pp. 91–95, 2009.

[23] S. P. Wang, J. G. Guo, and Y. Jiang, "The size- and chirality-dependent elastic properties of graphene nanofilms," *Journal of Computational and Theoretical Nanoscience*, vol. 10, no. 1, pp. 250–256, 2013.

[24] S. P. Wang, J. G. Guo, and L. J. Zhou, "Influence of Stone–Wales defects on elastic properties of graphene nanofilms," *Physica E: Low-dimensional Systems and Nanostructures*, vol. 48, pp. 29–35, 2013.

[25] H. Li and W. Guo, "Transversely isotropic elastic properties of single-walled carbon nanotubes by a rectangular beam model for the C-C bonds," *Journal of Applied Physics*, vol. 103, no. 10, article 103501, 2008.

[26] F. Scarpa, S. Adhikari, and A. Srikantha Phani, "Effective elastic mechanical properties of single layer graphene sheets," *Nanotechnology*, vol. 20, no. 6, 2009.

[27] K. I. Tserpes and P. Papanikos, "The effect of Stone–Wales defect on the tensile behavior and fracture of single-walled carbon nanotubes," *Composite Structures*, vol. 79, no. 4, pp. 581–589, 2007.

[28] T. Belytschko, S. P. Xiao, G. C. Schatz, and R. S. Ruoff, "Atomistic simulations of nanotube fracture," *Physical Review B*, vol. 65, no. 23, article 235430, 2002.

[29] C. Lee, X. Wei, J. W. Kysar, and J. Hone, "Measurement of the elastic properties and intrinsic strength of monolayer graphene," *Science*, vol. 321, no. 5887, pp. 385–388, 2008.

[30] F. Liu, P. Ming, and J. Li, "*Ab initio* calculation of ideal strength and phonon instability of graphene under tension," *Physical Review B*, vol. 76, no. 6, 2007.

[31] G. van Lier, C. van Alsenoy, V. van Doren, and P. Geerlings, "Ab initio study of the elastic properties of single-walled carbon nanotubes and graphene," *Chemical Physics Letters*, vol. 326, no. 1-2, pp. 181–185, 2000.

[32] R. Faccio, P. A. Denis, H. Pardo, C. Goyenola, and Á. W. Mombrú, "Mechanical properties of graphene nanoribbons," *Journal of Physics: Condensed Matter*, vol. 21, no. 28, article 285304, 2009.

[33] H. Zhao, K. Min, and N. R. Aluru, "Size and chirality dependent elastic properties of graphene nanoribbons under uniaxial tension," *Nano Letters*, vol. 9, no. 8, pp. 3012–3015, 2009.

[34] Y. Chu, T. Ragab, and C. Basaran, "The size effect in mechanical properties of finite-sized graphene nanoribbon," *Computational Materials Science*, vol. 81, no. 2, pp. 269–274, 2014.

[35] H. Yin, H. J. Qi, F. Fan, T. Zhu, B. Wang, and Y. Wei, "Griffith criterion for brittle fracture in graphene," *Nano Letters*, vol. 15, no. 3, pp. 1918–1924, 2015.

[36] Z. P. Bazant and J. Planas, *Fracture and Size Effect in Concrete and Other Quasibrittle Materials*, CRC Press, Boca Raton, FL, USA, 1997.

[37] A. A. Griffith, "The phenomena of rupture and flow in solids," *Philosophical Transactions of the Royal Society A: Mathematical, Physical and Engineering Sciences*, vol. 221, no. 582-593, pp. 163–198, 1921.

[38] M. Q. Le and R. C. Batra, "Crack propagation in pre-strained single layer graphene sheets," *Computational Materials Science*, vol. 84, no. 84, pp. 238–243, 2014.

[39] M. N. Ky and Y. J. Yum, "Mode I fracture toughness analysis of a single-layer grapheme sheet," *Journal of Mechanical Science and Technology*, vol. 28, no. 9, pp. 3645–3652, 2014.